A. Parrinello, K. Kesour, G.L. Ghiringhelli, N. Atalla
Diffuse Field Transmission Through Multilayered Cylinders Using a Transfer Matrix Method
Mechanical Systems and Signal Processing, Vol. 136, 2020, 106514 (13 pages)
doi:10.1016/j.ymssp.2019.106514

Diffuse Field Transmission through Multilayered Cylinders Using a Transfer Matrix Method

A. Parrinello[a,*], K. Kesour[a], G. L. Ghiringhelli[b], N. Atalla[a]

[a] *Université de Sherbrooke 2500, Boulevard de l'Université Sherbrooke (Québec) J1K 2R1*
[b] *Politecnico di Milano,Via La Masa 34, 20156 Milano, Italy*

Abstract

This paper discusses the use of a Transfer Matrix (TM) method for predicting the acoustic behavior of infinite cylinders consisting of a generic arrangement of homogeneous and heterogeneous periodic layers of various nature (fluid, solid, poroelastic). A through-radius TM is derived for a layer characterized by cylindrical periodicity by manipulating the dynamic stiffness matrix related to a finite element model of a unit cell. The proposed technique is equally appealing for homogeneous layers since few elements are needed in this case. In such a framework, different layers can be combined to form multilayered systems and the related acoustic radiation or transmission due to an external plane wave or a diffuse acoustic field can be assessed. The proposed approach is validated in case of cylinders consisting of homogeneous layers by comparison with alternative approaches. In order to demonstrate the usefulness of the approach, the sound transmission through a cylindrical structure with resonators is presented.

Keywords: Transfer Matrix Method, Infinite Cylinders, Diffuse Acoustic Field, Poroelastic Materials

*Corresponding author
Email address: andrea.parrinello@usherbrooke.ca (A. Parrinello)

1. Introduction

The sound transmission through infinite cylindrical structures is of importance in many industrial applications, e.g. pipes, launchers, aircraft fuselages and submarines. Usually, homogeneous layered media made up of lightweight poroelastic materials are employed in order to reduce the acoustic transmission into the interior cabin. The acoustic performance of such sound packages is poor at low frequencies. Recent use of structured materials, such as embedding resonant inclusions within a foam, has been proven effective to enhance the performance at low frequencies [1, 2, 3]. Various analytical and numerical tools are used to guide the design of these heterogeneous sound packages. However, most of the published work focuses on planar structures and the acoustic performance is usually assessed under normal incidence excitation. Due to the actual applications characteristics, computationally efficient design and optimization tools are still needed for more complex structures and excitations. This paper presents such a tool for the special case of an infinite cylindrical structure with attached heterogeneous sound packages under plane wave or diffuse acoustic field (DAF) excitations.

In this context, several works have studied the sound transmission through cylindrical structures using analytical models. For instance, Koval modeled analytically the sound transmission through a single isotropic as well as orthotropic cylindrical shell [4, 5] and extended the analysis to laminate composite shells [6] in the presence of an external mean flow. However, transverse shearing and rotational inertia were neglected in his studies. Later, Blaise and Lesueur [7, 8, 9] proposed an extension of Koval's work to handle acoustic transmission through isotropic and orthotropic multilayered cylindrical structures in order to compute the DAF transmission. Ghinet and Atalla [10] later proposed a more general alternative for modeling the transmission loss (TL) through infinite laminated and sandwich composite shells. In their model, the transverse shearing and rotational inertia as well as the orthotropic ply angle were considered. In a recent paper, Magniez et al. [11] proposed a 3D-shell analytical model and applied it

to assess the plane wave transmission through a cylinder composed of two thin orthotropic skins and a thick isotropic core. Later, they developed a sandwich shell model which take into account the elasticity effect of a poroelastic core by means of the Biot model [12]. However, the coupling effect between the poroelastic material and the two skins was not studied in their work. Other recent works studied the aforementioned coupling effect in the case of an oblique incidence angle [13, 14, 15, 16] as well as a DAF [17]. However, the poroelastic material was modeled as an equivalent fluid based on the methodology proposed by Lee et al. [18].

The characterization of wave propagation in complex structures using a wave and finite element method (WFEM) has also received a lot of attention. The WFEM combines conventional Finite Element (FE) and the theory of wave propagation in periodic structures making it possible to overcome the complex algebra expressions involved in the development of analytical models. Mencik and Ichchou [19] used a one-dimensional WFEM to find the dispersion curve and the forced response of an infinite cylinder filled with acoustic fluid. Manconi and Mace [20, 21] developed a two-dimensional WFEM to compute the dispersion curve of curved and cylindrical structures. Later, Renno and Mace [22] extended the two-dimensional WFEM to calculate a forced response of a cylinder in vacuo. The cylinder's axisymmetry was exploited. Chronopoulos [23] proposed a 2D WFEM to predict the dispersion characteristics of composite orthotropic curved panels and cylindrical shell structures as well as the TL within a statistical energy framework. In addition, Errico et al. [24] used a 1D axisymmetric WFEM, within a Transfer Matrix (TM) framework, to model the flow-induced vibrations of periodic and axisymmetric structures when random spatially correlated loads acting on the external surface. Periodic cylinders and curved panels under turbulent boundary layer and DAF excitations are also considered in [25]. Droz et al. [26] used small-scale resonators combined with poroelastic foam to improve the TL around the ring frequency. Recently, Kingan et al. [27] modeled the sound transmission through cylindrical structures using a two-dimensional WFEM. In their work, the infinite cylindrical structure is

excited by a point source. None of the above papers tackle cylinders with attached heterogeneous sound packages. In addition, equally important and to the authors knowledge, only few recent papers deal with the transmission through sandwich cylinders with a poroelastic core [28, 29]. The latter are however based on analytical formulations that limiting them to homogeneous cases.

This paper alleviates these limitations using an approach based on the WFEM. An extension of a TM representation defined for periodic planar media by a FE model of a periodic unit cell (UC) [30] is presented. Main additions to [30] consist in the modification of the dynamic stiffness matrix (DSM) of the UC to account for the curvature and in the boundary conditions with external and internal fluids, including the excitation, which are modeled analytically. Moreover, multilayered cylinders consisting of a generic arrangement of heterogeneous fluid, solid and poroelastic layers are considered. The layers' transfer matrices are then used in a TM context to predict sound transmission through the cylinders in case of a single oblique plane wave excitation or a DAF excitation. The method is easily applicable to other type of excitation using appropriate k-wave decompositions; for example for a point source in the exterior domain, the Sommerfeld decomposition can be used to represent the monopole field in terms of plane waves and thus use the same methodology of the paper to compute the TL; an example for a planar structure is given in chapter 7 of reference [31].

This paper is composed of two parts. In the first, the theoretical steps used to derive the proposed approach are presented. The modeling of the plane wave excitation and the coupling with external and internal fluid media are recalled, then the transfer matrix of a layer is derived, finally the global system is assembled and the TL is evaluated. In the second part, the proposed approach is validated first in case of cylinders consisting of homogeneous layers by comparison with alternative approaches. Then, several examples are presented to illustrate the practical use of the approach. In particular, an application to the prediction of the TL of a cylindrical structure with attached or embedded resonators is discussed.

2. Theory

Let us consider the infinite multilayered cylinderdepicted in Figure 1. The cylinder longitudinal axis lies along the X-axis and its inner and outer surfaces are respectively located at $r = r_i$ and $r = r_o$. Subscripts i and o indicating values at the inner and outer surfaces or properties of the internal and external fluids. The fluid pressures on the inner and outer surfaces are thus denoted $p_{i,o}$. The fluids have densities and wave speeds $\rho_{i,o}$ and $c_{i,o}$ respectively. Throughout the analysis we assume time-harmonic motion of the form $\exp(\mathrm{j}\omega t)$.

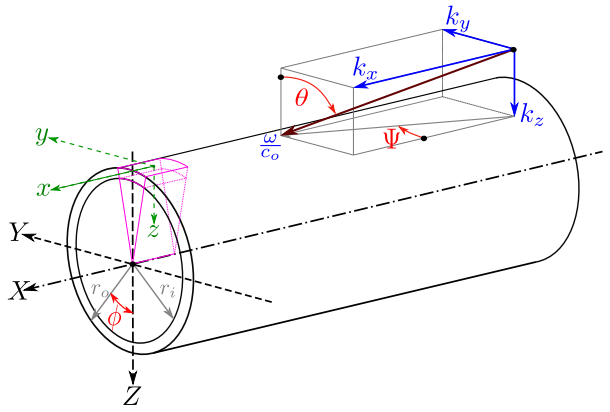

Figure 1: Infinite cylinder excited by an oblique plane wave.

2.1. Acoustic Excitation and Impedances

In this section the analytical modeling of the incident and transmitted fields is recalled. Details can be found in references [7, 10, 17, 27]. The cylinder is excited by an external oblique plane wave with an incident angle, $\theta \in [0\ \pi/2]$, with respect to the radial direction and a heading angle, $\Psi \in [0\ 2\pi)$, with respect to the cylinder axis as depicted in Figure 1.

The incident pressure field (plane wave) can be expressed in cylindrical harmonics using the Jacobi-Anger expansion as [32]

$$P_I = p_0 e^{\mathrm{j}(\omega t - k_x x - k_y y - k_z z)} = p_0 e^{\mathrm{j}(\omega t - k_x x)} \sum_{n=0}^{\infty} \varepsilon_n (-\mathrm{j})^n J_n(k_o r) \cos(n(\phi + \beta)) \ , \tag{1}$$

where p_0 is the wave amplitude, k_x and k_o are the wavenumber components

$$\begin{cases} k_x = \dfrac{\omega}{c_o} \sin\theta \cos\Psi \\ k_o = \sqrt{\left(\dfrac{\omega}{c_o}\right)^2 - k_x^2} = \dfrac{\omega}{c_o} \dfrac{\cos\theta}{\cos\beta} \end{cases} , \tag{2}$$

c_o is the speed of sound of the external fluid, the auxiliary angle $\beta \in [0\ \pi/2)$ is defined as [7]

$$\tan\beta = \tan\theta\ \sin\Psi\ , \tag{3}$$

n is the circumferential mode number, ε_n is the Neumann factor ($\varepsilon_n = 1$ if $n = 0$, $\varepsilon_n = 2$ if $n > 0$) and J_n is the Bessel function of order n. The pressure field in the external fluid due to the reflection at the outer surface of the cylinder is given by

$$P_R = e^{\mathrm{j}(\omega t - k_x x)} \sum_{n=0}^{\infty} A_n H_n^{(2)}(k_o r) \cos(n(\phi + \beta))\ , \tag{4}$$

where A_n is the n-th complex amplitude and $H_n^{(2)}$ is the Hankel function of second kind of order n. The total pressure field in the external fluid is equal to $P_I + P_R$. The *blocked-wall* pressure, P_B, (*i.e.* the real excitation seen by the cylinder) is obtained by assuming a Neumann boundary at $r = r_o$, thus obtaining the amplitude factors A_n and the total (blocked) pressure at the outer surface produced by the incident plane wave [17]:

$$P_B = p_0 e^{\mathrm{j}(\omega t - k_x x)} \sum_{n=0}^{\infty} \varepsilon_n (-\mathrm{j})^n \left[J_n(k_o r_o) - \frac{H_n^{(2)}(k_o r_o) J_n'(k_o r_o)}{H_n^{(2)'}(k_o r_o)} \right] \cos(n(\phi + \beta))\ , \tag{5}$$

where $f'(x) = \mathrm{d}f/\mathrm{d}x$.

The spectral pressure acting on the outer surface of the cylinder due to the outer (inward-pointing) radial spectral velocity, $v_{o,n}$, is given by $p_{o,n} = -Z_{o,n} v_{o,n}$ where

$$Z_{o,n} = -\frac{\mathrm{j}\omega\rho_o}{k_o} \frac{H_n^{(2)}(k_o r_o)}{H_n^{(2)'}(k_o r_o)} \tag{6}$$

is the acoustic impedance at the outer surface [27]. In case of a non-resonant cavity (with only inward propagating waves), the spectral pressure acting on

the inner surface due to the inner (inward-pointing) radial spectral velocity, $v_{i,n}$, can be expressed as $p_{i,n} = Z_{i,n} v_{i,n}$ where

$$Z_{i,n} = \frac{\mathrm{j}\omega\rho_i}{k_i} \frac{H_n^{(1)}(k_i r_i)}{H_n^{(1)'}(k_i r_i)} \tag{7}$$

is the acoustic impedance at the inner surface [27], $H_n^{(1)}$ is the Hankel function of first kind of order n and $k_i = \sqrt{(\omega/c_i)^2 - k_x^2}$ is the radial component of the wavenumber in the internal fluid. Even though only non-resonant cavities are considered in this work, the acoustic impedance at the inner surface in case of a resonant cavity [27] is here reported for sake of completeness:

$$Z_{i,n} = \frac{\mathrm{j}\omega\rho_i}{k_i} \frac{J_n(k_i r_i)}{J_n'(k_i r_i)} \ . \tag{8}$$

2.2. Transfer Matrix of a Periodic Layer

In order to simplify the following presentation, only layers defined by a single physics (solid, fluid or porous) at the inter-layer boundaries are considered. Details on the mixed formulation can be found in [30]. Moreover, models of porous media are not discussed, they can can be found in [31]. The presented approach is general: different physics are allowed for within a layer and different materials with the same physics are allowed for at the inter-layer boundaries.

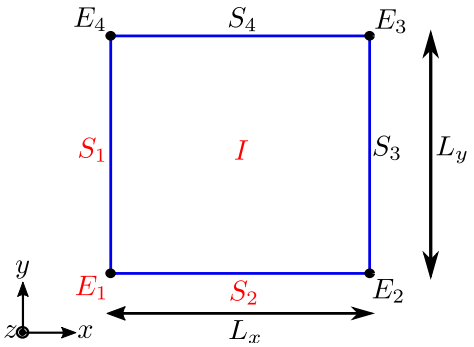

Figure 2: Unit cell (in local coordinates $x-y-z$) partitioned into internal region (I), surfaces S_{1-4} and edges E_{1-4}. The reduced problem involves only I, S_1, S_2, E_1.

The periodic UC of a layer is represented by a straight cuboid as depicted in Figure 2. The reference coordinates system $(x - y - z)$ of the selected UC

is parallel to the reference coordinates system $(X-Y-Z)$ of the cylinder as depicted in Figure 1. As a consequence, the local z-axis of the UC corresponds to the inward-pointing radial direction. The periodic UC of a layer is modeled using FEs and the related dynamic problem can be written as

$$\bar{\mathbf{D}}(\omega)\mathbf{q} = \mathbf{f} + \mathbf{e} \ , \tag{9}$$

where $\bar{\mathbf{D}}(\omega)$ is the DSM of the UC, $\mathbf{q}$ is the vector of generalized displacements or pressures, $\mathbf{f}$ is the vector of generalized internal forces, *i.e.* due to adjacent UCs, and $\mathbf{e}$ is the vector of generalized external forces, *i.e.* due to bounding media. In case of a solid or porous layer, the local coordinates of the FE model must be rotated in order to account for the desired curvature. The modified DSM is defined as

$$\mathbf{D} = \mathbf{R}^T \bar{\mathbf{D}} \mathbf{R} \ , \tag{10}$$

where $\mathbf{R}$ is a block diagonal matrix. In case of a solid layer the i-th block of matrix $\mathbf{R}$ is defined as

$$\mathbf{R}_i = \begin{bmatrix} 1 & 0 & 0 \\ 0 & \cos\alpha_i & \sin\alpha_i \\ 0 & -\sin\alpha_i & \cos\alpha_i \end{bmatrix} \ , \tag{11}$$

where $\alpha_i = y_i/R$, y_i is the y-axis coordinate of the i-th node of the solid phase and $R = (r_i + r_o)/2$ is the mean radius. In the context of a mixed displacement-pressure formulation for porous materials [33], the i-th block of matrix $\mathbf{R}$ is defined as

$$\mathbf{R}_i = \begin{bmatrix} 1 & 0 & 0 & 0 \\ 0 & \cos\alpha_i & \sin\alpha_i & 0 \\ 0 & -\sin\alpha_i & \cos\alpha_i & 0 \\ 0 & 0 & 0 & 1 \end{bmatrix} \ . \tag{12}$$

In order to apply periodic boundary conditions, the UC is partitioned in internal region (I), four surfaces (S_{1-4}) and four edges (E_{1-4}) as depicted in Figure 2. Bloch's theorem must be applied to the generalized displacements vector as

$$\mathbf{q} = \left(\mathbf{\Lambda}_0 + \mathbf{\Lambda}_x e^{\mathrm{j}k_x L_x} + \mathbf{\Lambda}_y e^{\mathrm{j}k_y L_y} + \mathbf{\Lambda}_{xy} e^{\mathrm{j}(k_x L_x + k_y L_y)} \right) \mathbf{q}' = \mathbf{A}\mathbf{q}' \ , \tag{13}$$

where $\mathbf{\Lambda}_X$ are linear interpolation matrices linking nodal displacements and pressures at the slave boundaries (S_{3-4}, E_{2-4}) to the nodal values at the master

boundaries (S_{1-2}, E_1), the longitudinal wavenumber, k_x, is defined in Eq. (2), $k_y = n/R$ is the tangential wavenumber and (L_x, L_y) are the UC dimensions. Interpolation matrices allow to handle UCs with different meshes at opposite boundaries, making the procedure less restrictive in terms of mesh requirements. Thus, the equation of motion, Eq. (9), can be reduced as

$$\mathbf{A}^H \mathbf{D}(\omega) \mathbf{A} \mathbf{q}' = \mathbf{D}'(\omega, k_x, k_y) \mathbf{q}' = \mathbf{A}^H (\mathbf{f} + \mathbf{e}) \ . \tag{14}$$

Under the assumption of real wavenumbers, the forces due to neighboring cells disappear from the dynamic problem [30] and the equation of motion becomes

$$\mathbf{D}'(\omega, k_x, k_y) \mathbf{q}' = \mathbf{e}' \ . \tag{15}$$

In order to evaluate the TM of the layer, the problem must be partitioned in terms of top (T), bottom (B) and internal (I) sets. Since no internal forces are applied, the set of internal degrees of freedom (dofs), $\mathbf{q}'_I$, can be removed and the problem can be arranged as

$$\begin{bmatrix} \mathbf{D}'_{BB} - \mathbf{D}'_{BI} \mathbf{D}_{II}^{'-1} \mathbf{D}'_{IB} & \mathbf{D}'_{BT} - \mathbf{D}'_{BI} \mathbf{D}_{II}^{'-1} \mathbf{D}'_{IT} \\ \mathbf{D}'_{TB} - \mathbf{D}'_{TI} \mathbf{D}_{II}^{'-1} \mathbf{D}'_{IB} & \mathbf{D}'_{TT} - \mathbf{D}'_{TI} \mathbf{D}_{II}^{'-1} \mathbf{D}'_{IT} \end{bmatrix} \begin{Bmatrix} \mathbf{q}'_B \\ \mathbf{q}'_T \end{Bmatrix} = \mathbf{C}' \begin{Bmatrix} \mathbf{q}'_B \\ \mathbf{q}'_T \end{Bmatrix} = \begin{Bmatrix} \mathbf{e}'_B \\ \mathbf{e}'_T \end{Bmatrix} . \tag{16}$$

Note that all the inversions in Eq. (16) can be handled with a single LU factorization. This factorization represents the main computational bottleneck of the method. However, homogeneous layers can be modeled by means of UCs with no internal nodes, thus avoiding the above mentioned factorization and the related cost. Such a possibility ensures to the proposed procedure a computational efficiency akin to analytical formulations.

To build the corresponding one dimensional TM model, we first define the matrices

$$\mathbf{L}_B = \mathbf{I}_m \otimes \exp(\mathrm{j} k_x \mathbf{x}_B + \mathrm{j} k_y \mathbf{y}_B) \ , \ \mathbf{L}_T = \mathbf{I}_m \otimes \exp(\mathrm{j} k_x \mathbf{x}_T + \mathrm{j} k_y \mathbf{y}_T) \ , \tag{17}$$

where $\mathbf{x}|\mathbf{y}_{B|T}$ are row vectors collecting nodal coordinates, $\mathbf{I}_m$ is the identity matrix of size m, m is the number of dofs for each node (1 for fluid and equivalent fluid layers, 3 for solid layers, 4 for poroelastic layers [33]) and $\otimes$ denotes

the Kronecker product. Thus, the through-thickness one dimensional dynamic problem can be derived:

$$\begin{bmatrix} \mathbf{L}_B\mathbf{C}'_{BB}\mathbf{L}_B^H & \mathbf{L}_B\mathbf{C}'_{BT}\mathbf{L}_T^H \\ \mathbf{L}_T\mathbf{C}'_{TB}\mathbf{L}_B^H & \mathbf{L}_T\mathbf{C}'_{TT}\mathbf{L}_T^H \end{bmatrix} \begin{Bmatrix} \hat{\mathbf{q}}_B \\ \hat{\mathbf{q}}_T \end{Bmatrix} = \mathbf{C} \begin{Bmatrix} \hat{\mathbf{q}}_B \\ \hat{\mathbf{q}}_T \end{Bmatrix} = \begin{Bmatrix} \hat{\mathbf{e}}_B \\ \hat{\mathbf{e}}_T \end{Bmatrix} \ . \tag{18}$$

Finally, the problem can be rearranged in terms of a transfer matrix:

$$\begin{bmatrix} -\mathbf{C}_{TB}^{-1}\mathbf{C}_{TT} & \mathbf{C}_{TB}^{-1} \\ \mathbf{C}_{BT} - \mathbf{C}_{BB}\mathbf{C}_{TB}^{-1}\mathbf{C}_{TT} & \mathbf{C}_{BB}\mathbf{C}_{TB}^{-1} \end{bmatrix} \begin{Bmatrix} \hat{\mathbf{q}}_T \\ \hat{\mathbf{e}}_T \end{Bmatrix} = \mathbf{T}'(\omega, k_x, k_y) \begin{Bmatrix} \hat{\mathbf{q}}_T \\ \hat{\mathbf{e}}_T \end{Bmatrix} = \begin{Bmatrix} \hat{\mathbf{q}}_B \\ \hat{\mathbf{e}}_B \end{Bmatrix} \ . \tag{19}$$

It should be noted that matrix $\mathbf{C}_{TB}$ is very small ($m \times m$), so the cost related to its inversion is negligible within the procedure.

The transfer matrix $\mathbf{T}'$ is now modified in order to simplify the inter-layer boundary conditions. Using transformation matrices $\mathbf{\Lambda}_T$ and $\mathbf{\Lambda}_B$ (defined below), new state vectors, $\mathbf{V}_T$ and $\mathbf{V}_B$, are related to the original state vectors, $\mathbf{V}'_T = [\hat{\mathbf{q}}_T \ \ \hat{\mathbf{e}}_T]^T$ and $\mathbf{V}'_B = [\hat{\mathbf{q}}_B \ \ \hat{\mathbf{e}}_B]^T$ as

$$\mathbf{V}'_T = \mathbf{\Lambda}_T\mathbf{V}_T \ , \ \mathbf{V}_B = \mathbf{\Lambda}_B\mathbf{V}'_B \ , \tag{20}$$

thus obtaining the final form of the transfer matrix as

$$\mathbf{T} = \mathbf{\Lambda}_B\mathbf{T}'\mathbf{\Lambda}_T \ . \tag{21}$$

The original and the chosen state vectors for a fluid layer are respectively

$$\mathbf{V}'_f = \begin{bmatrix} p & -\mathrm{j}\omega A v_n^f \end{bmatrix}^T \ , \ \mathbf{V}_f = \begin{bmatrix} p & v_z^f \end{bmatrix}^T \tag{22}$$

where v_n^f is the (outward-pointing) normal velocity and $A = L_xL_y$ is the area of the UC. As a consequence, the related transformation matrices are

$$\mathbf{\Lambda}_B = \mathrm{diag}\begin{bmatrix} 1 & 1/\mathrm{j}\omega A \end{bmatrix} \ , \ \mathbf{\Lambda}_T = \mathrm{diag}\begin{bmatrix} 1 & -\mathrm{j}\omega A \end{bmatrix} \ . \tag{23}$$

The state vectors for a solid layer are

$$\mathbf{V}'_s = \begin{bmatrix} u_x & u_y & u_z & F_x & F_y & F_z \end{bmatrix}^T \ , \ \mathbf{V}_s = \begin{bmatrix} v_x^s & v_y^s & v_z^s & \sigma_{zx} & \sigma_{zy} & \sigma_{zz} \end{bmatrix}^T \tag{24}$$

and the related transformation matrices are

$$\begin{aligned}\mathbf{\Lambda}_B &= \mathrm{diag}\begin{bmatrix}\mathrm{j}\omega & \mathrm{j}\omega & \mathrm{j}\omega & -1/A & -1/A & -1/A\end{bmatrix}\ ,\\ \mathbf{\Lambda}_T &= \mathrm{diag}\begin{bmatrix}1/\mathrm{j}\omega & 1/\mathrm{j}\omega & 1/\mathrm{j}\omega & A & A & A\end{bmatrix}\ .\end{aligned} \tag{25}$$

The state vector related to the used poroelastic formulation [33] is

$$\mathbf{V}'_p = \begin{bmatrix}u_x^s & u_y^s & u_z^s & p & F_x^s & F_y^s & F_z^s & -\mathrm{j}\omega A(v_n^f + v_n^s\tilde{\gamma}/\Phi^2)\end{bmatrix}^T \tag{26}$$

where Φ is the layer porosity and $\tilde{\gamma}$ is a coupling coefficient between the solid and fluid phase of the porous media. On the other hand, the chosen state vector is

$$\mathbf{V}_p = \begin{bmatrix}v_x^s & v_y^s & v_z^s & p & \sigma_{zx}^s & \sigma_{zy}^s & \sigma_{zz}^t & w\end{bmatrix}^T \tag{27}$$

where $w = \Phi(v_z^f - v_z^s)$ is the flux per unit area at the interface, $\sigma_{zz}^t = \sigma_{zz}^s + \sigma_{zz}^f$ is the total normal stress and $\sigma_{zz}^f = -p\Phi$ is the equivalent normal stress due to the fluid. The related transformation matrices are

$$\mathbf{\Lambda}_T = \left[\begin{array}{cccc|cccc} 1/\mathrm{j}\omega & 0 & 0 & 0 & 0 & 0 & 0 & 0\\ 0 & 1/\mathrm{j}\omega & 0 & 0 & 0 & 0 & 0 & 0\\ 0 & 0 & 1/\mathrm{j}\omega & 0 & 0 & 0 & 0 & 0\\ 0 & 0 & 0 & 1 & 0 & 0 & 0 & 0\\ 0 & 0 & 0 & 0 & A & 0 & 0 & 0\\ 0 & 0 & 0 & 0 & 0 & A & 0 & 0\\ 0 & 0 & 0 & \Phi A & 0 & 0 & A & 0\\ 0 & 0 & -gA & 0 & 0 & 0 & 0 & -\mathrm{j}\omega A/\Phi \end{array}\right] \tag{28}$$

and

$$\mathbf{\Lambda}_B = \left[\begin{array}{cccc|cccc} \mathrm{j}\omega & 0 & 0 & 0 & 0 & 0 & 0 & 0\\ 0 & \mathrm{j}\omega & 0 & 0 & 0 & 0 & 0 & 0\\ 0 & 0 & \mathrm{j}\omega & 0 & 0 & 0 & 0 & 0\\ 0 & 0 & 0 & 1 & 0 & 0 & 0 & 0\\ 0 & 0 & 0 & 0 & -1/A & 0 & 0 & 0\\ 0 & 0 & 0 & 0 & 0 & -1/A & 0 & 0\\ 0 & 0 & 0 & -\Phi & 0 & 0 & -1/A & 0\\ 0 & 0 & -g\Phi & 0 & 0 & 0 & 0 & \Phi/\mathrm{j}\omega A \end{array}\right] \tag{29}$$

where $g = \mathrm{j}\omega(1 + \tilde{\gamma}/\Phi^2)$.

2.3. Assembling and Solution

This section is devoted to the continuity conditions between adjacent layers. In case of a solid-fluid interface the following conditions must be imposed

$$\mathbf{I}_{sf}\mathbf{V}_s + \mathbf{J}_{sf}\mathbf{V}_f = \left[\begin{array}{cc|cccc} 0 & 0 & 1 & 0 & 0 & 0\\ 0 & 0 & 0 & 1 & 0 & 0\\ 0 & 0 & 0 & 0 & 1 & 0\\ 0 & 0 & 0 & 0 & 0 & 1 \end{array}\right]\mathbf{V}_s + \begin{bmatrix} 0 & -1\\ 0 & 0\\ 0 & 0\\ 1 & 0 \end{bmatrix}\mathbf{V}_f = \mathbf{0}\ . \tag{30}$$

Matrices $\mathbf{I}_{sf}$ and $\mathbf{J}_{sf}$ must be interchanged for a fluid-solid interface. The state vector $\mathbf{V}_p$ defined by Eq. (27) considerably simplify the porous-porous and the porous-fluid interfaces, making interface conditions independent from the porosity, Φ. In fact, all the components of $\mathbf{V}_p$ are equal at each side of the boundary between two porous layers with frames bonded together. On the other hand, the following boundary conditions must be set for a porous-fluid interface

$$\mathbf{I}_{pf}\mathbf{V}_p+\mathbf{J}_{pf}\mathbf{V}_f = \left[\begin{array}{cc|ccccc|c} 0 & 0 & 1 & 0 & 0 & 0 & 0 & 1 \\ 0 & 0 & 0 & 1 & 0 & 0 & 0 & 0 \\ 0 & 0 & 0 & 0 & 1 & 0 & 0 & 0 \\ 0 & 0 & 0 & 0 & 0 & 1 & 0 & 0 \\ 0 & 0 & 0 & 0 & 0 & 0 & 1 & 0 \end{array}\right] \mathbf{V}_p+ \begin{bmatrix} 0 & -1 \\ -1 & 0 \\ 0 & 0 \\ 0 & 0 \\ 1 & 0 \end{bmatrix} \mathbf{V}_f = \mathbf{0} \ . \quad (31)$$

Matrices $\mathbf{I}_{pf}$ and $\mathbf{J}_{pf}$ must be interchanged for a fluid-porous interface. In case of a porous-solid interface the following boundary conditions must be set

$$\mathbf{I}_{ps}\mathbf{V}_p + \mathbf{J}_{ps}\mathbf{V}_s = \begin{bmatrix} [\mathbf{I}_3 & \mathbf{0}] \\ [\mathbf{0} & \mathbf{I}_4] \end{bmatrix} \mathbf{V}_p + \begin{bmatrix} -\mathbf{I}_6 \\ \mathbf{0} \end{bmatrix} \mathbf{V}_s = \mathbf{0} \ , \quad (32)$$

where $\mathbf{I}_n$ is the identity matrix of size n. Matrices $\mathbf{I}_{ps}$ and $\mathbf{J}_{ps}$ must be interchanged for a solid-porous interface.

If two or more adjacent layers have the same nature (including porous layers) the global transfer matrix is simply equal to the product of the transfer matrices of the layers. Alternatively, if two adjacent layers, i and j, are defined by the same state vector $\mathbf{V}_{i|j}$ of size n, the interface matrices $\mathbf{I}_{ij} = \mathbf{I}_n$ and $\mathbf{J}_{ij} = -\mathbf{I}_n$ can be used to fulfill continuity conditions, thus retaining the state variables at the i-j interface.

Stacking all the continuity conditions we obtain

$$\mathbf{BV} = \begin{bmatrix} \mathbf{I}_{f1} & \mathbf{J}_{f1}\mathbf{T}_1 & \mathbf{0} & \cdots & \mathbf{0} & \mathbf{0} \\ \mathbf{0} & \mathbf{I}_{12} & \mathbf{J}_{12}\mathbf{T}_2 & \cdots & \mathbf{0} & \mathbf{0} \\ \vdots & \vdots & \vdots & \ddots & \vdots & \vdots \\ \mathbf{0} & \mathbf{0} & \mathbf{0} & \cdots & \mathbf{I}_{lf} & \mathbf{J}_{lf} \\ \mathbf{0} & \mathbf{0} & \mathbf{0} & \cdots & \mathbf{0} & -1 \quad Z_i \end{bmatrix} \begin{Bmatrix} p_o \\ v_o^f \\ \vdots \\ p_i \\ v_i^f \end{Bmatrix} = \mathbf{0} \ , \quad (33)$$

where matrix $\mathbf{B}$ has dimensions $N \times (N+1)$, matrices $\mathbf{I}_{ij}$ and $\mathbf{J}_{ij}$ depend on the nature of the i-th and j-th layers, l is the number of layers, the suffix f denotes

the fluid at the excitation and termination side and impedance condition is imposed at the termination side by means of the inner impedance, Z_i. The global state vector, $\mathbf{V}$, collects the variables at all interfaces only if interface matrices are employed even for adjacent layers of the same nature. Impedance condition and spectral blocked pressure must also be applied at the excitation (outer) side

$$\mathbf{B}_{2:N+1}\mathbf{V}_{2:N+1} = -\mathbf{B}_1 p_o = -\mathbf{B}_1 \left(p_B - Z_o v_o^f\right) \ , \tag{34}$$

where $\mathbf{B}_i$ is the i-th column of matrix $\mathbf{B}$ and $\mathbf{B}_{i:j}$ is the matrix ranging from the i-th to the j-th column of $\mathbf{B}$. The problem can be rearranged by obtaining a square linear system with N unknowns:

$$\begin{bmatrix}\mathbf{B}_2 - Z_o\mathbf{B}_1 & \mathbf{B}_{3:N+1}\end{bmatrix}\mathbf{V}_{2:N+1} = -\mathbf{B}_1 p_B \ , \tag{35}$$

where v_o^f and v_i^f are the first and the last element of vector $\mathbf{V}_{2:N+1}$ respectively.

Once fluid velocities at boundaries are determined, the power transmission coefficient can be evaluated. The incident acoustic power per unit length on the outer surface of the cylinder ($r = r_o$) is given by

$$W_I(\omega,\theta,\Psi) = \frac{p_0^2 r_o \cos\theta}{\rho_o c_o \cos\beta} \ . \tag{36}$$

On the other hand, the transmitted sound power per unit length of the inner surface ($r = r_i$) is [17]

$$\begin{aligned} W_T(\omega,\theta,\Psi) &= \sum_{n=0}^{\infty} \frac{r_i}{2}\Re\left[p_{i,n}(v_{i,n}^f)^H\right]\int_0^{2\pi}\cos^2(n(\phi+\beta))\mathrm{d}\phi \\ &= \sum_{n=0}^{\infty}\frac{\pi r_i}{\varepsilon_n}\Re(Z_{i,n})|v_{i,n}^f|^2 \ . \end{aligned} \tag{37}$$

Thus, the power transmission coefficient is defined as

$$\tau(\omega,\theta,\Psi) = \frac{W_T(\omega,\theta,\Psi)}{W_I(\omega,\theta,\Psi)} = \frac{\pi\rho_o c_o r_i\cos\beta}{p_0^2 r_o\cos\theta}\sum_{n=0}^{\infty}\frac{\Re(Z_{i,n})|v_{i,n}^f|^2}{\varepsilon_n} \ . \tag{38}$$

In the case of a DAF excitation, the transmission coefficient is expressed as

$$\tau_d(\omega) = \frac{\int_0^{2\pi}\int_{\theta_{\min}}^{\theta_{\max}}\tau(\omega,\theta,\Psi)\cos\theta\sin\theta\,\mathrm{d}\theta\,\mathrm{d}\Psi}{\int_0^{2\pi}\int_{\theta_{\min}}^{\theta_{\max}}\cos\theta\sin\theta\,\mathrm{d}\theta\,\mathrm{d}\Psi} \ , \tag{39}$$

where $\theta_{\min}$ and $\theta_{\max}$ are the minimum and maximum angles of incidence, respectively [34]. Finally, the TL is defined as

$$\mathrm{TL} = -10 \log_{10}(\tau_d) \ . \tag{40}$$

In case of a planar structure and identical inner and outer fluids we obtain: $p_B = 2p_0$, $Z_i = \rho_i c_i / \cos\theta$, $Z_o = \rho_o c_o / \cos\theta$ and

$$\tau(\omega, \theta, \Psi) = \frac{Z_i Z_o}{p_0^2} |v_i^f|^2 \ . \tag{41}$$

3. Results

In this section several examples are used to illustrate the validity and applications of the proposed approach. Cylinders with both homogeneous and heterogeneous layers are considered. In case of a homogeneous layer a cubic periodic unit consisting of one hexa8 element (solids) or five tetra4 elements (fluids or porous) is used to define the TM of the layer. The height of the cube is selected as a fraction of the layer ($h_{\text{cube}} = h_{\text{layer}}/N_z$) and the TM of the layer is recovered as power of the elementary one ($\mathbf{T}_{\text{layer}} = \mathbf{T}_{\text{cube}}^{N_z}$). Such a selection ensures high efficiency for homogeneous layers. The fluids properties are $c_i = c_o = 340$ ms^{-1} and $\rho_i = \rho_o = 1.284$ kgm^{-3} for all the cases. To ensure convergence, at each frequency and incident plane wave, the number of harmonics is incremented till $|\tau_j - \tau_{j-1}|/\tau_j > 10^{-5}$, where $\tau_j = \sum_{n=0}^{j} \tau_n$.

To validate the presented approach, we consider two configurations involving homogeneous layers. The first case concerns the diffuse field TL through an infinite cylinder ($R = 2$ m) consisting of a 3 mm thick steel layer ($N_z = 20$). The steel has properties: $E = 210$ GPa, $\nu = 0.3$, $\mu = 0.1$ %, $\rho = 7800$ kgm^{-3}. Figure 3 presents the comparison of the TL predicted by the proposed approach (TMM) with the result produced by an analytical model [10]. An excellent agreement is observed between the methods over the whole frequency range.

The second case concerns an infinite sandwich cylinder consisting of 2 mm thick orthotropic skins ($N_z = 20$) and 50 mm thick foam core ($N_z = 80$). The skins have properties: $E_x = 137.9$ GPa, $E_y = E_z = 8.96$ GPa, $G_{yz} = 6.2$ GPa,

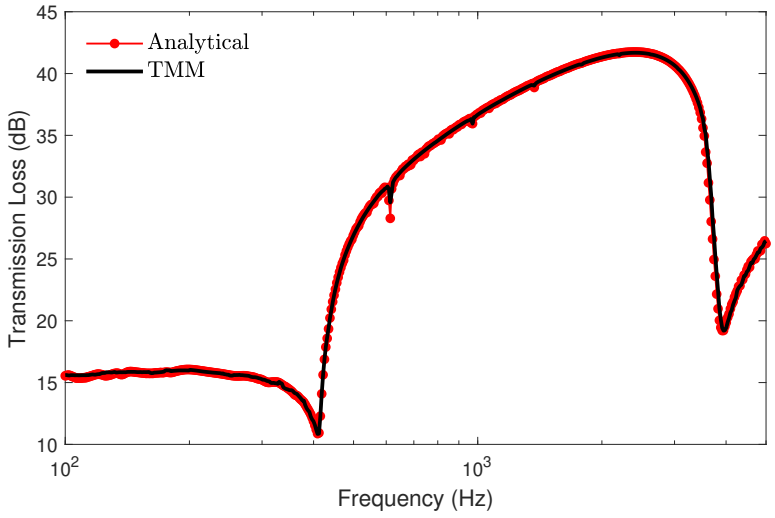

Figure 3: TL for DAF excitation through a 3 mm thick steel cylinder ($R = 2$ m).

$G_{xy} = G_{xz} = 7.1$ GPa, $\nu_{xy} = \nu_{xz} = 0.3$, $\mu = 0$ %, $\rho = 1600$ kgm^{-3}. The foam has properties: $\Phi = 0.994$, $\sigma = 9045$ Nsm^{-4}, $\alpha_\infty = 1.02$, $\Lambda = 103$ μm, $\Lambda' = 197$ μm, $E = 194.9$ kPa, $\nu = 0.42$, $\mu = 5$ %, $\rho = 8.43$ kgm^{-3}. The cylinder has external radius $r_o = 2.164$ m and internal radius $r_i = 2.11$ m. Figure 4 compares the TL at oblique incidence ($\theta = 45°$, $\Psi = 0°$) predicted by the proposed approach (TMM) with the result produced by an alternative approach based on a WFEM applied to a periodic UC of the multilayered cylinder (PUC) and also with the result produced by an analytical model [28]. An excellent agreement is observed between all methods over the whole frequency range.

To illustrate the ease of handling various interface conditions in the presented approach, the case in which the foam fills the gap between the two skins (BB) is now compared to two configurations in which air gaps are interposed between the foam and the skins. Air gaps of $\delta = 10$ mm and $\delta/2$ are used in the BU and UU configurations, respectively, as depicted in Figure 5. Figure 6 presents the TLs of the three configurations in case of a DAF excitation. BU and UU configurations provide higher TL with respect to the BB configuration in the frequency range which spans form the ring frequency to the critical frequency

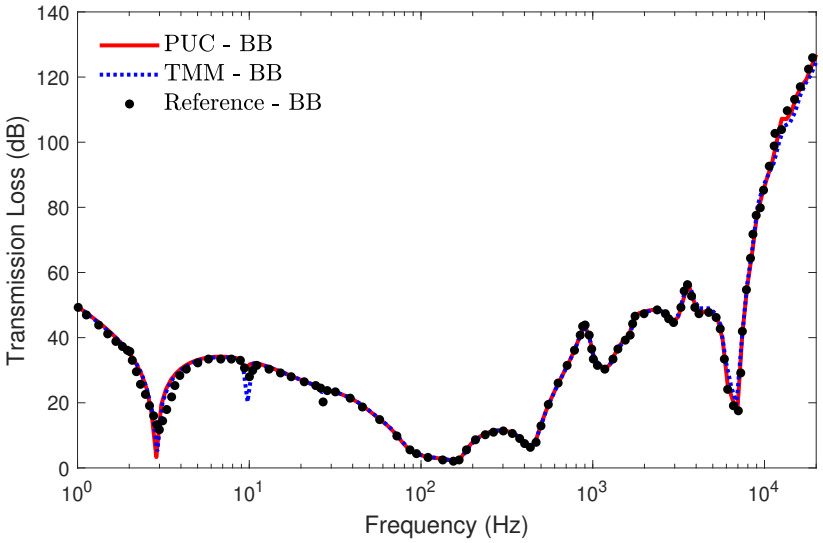

Figure 4: TL at oblique incidence ($\theta = 45°$,$\Psi = 0°$) through an orthotropic sandwich cylinder ($R = 2.156$ m).

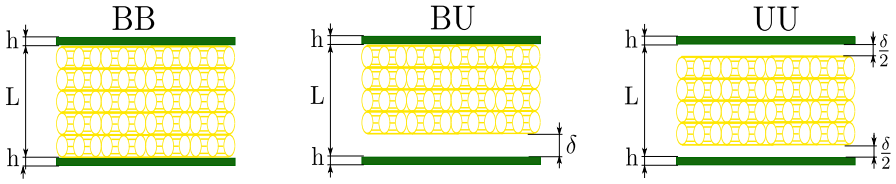

Figure 5: Configurations of a sandwich cylinder.

because of the shear decoupling between the skins and the core ensured by the air gaps.

The next case illustrates the validity of using the Insertion Loss (IL) evaluated for a flat structure to assess the TL of a cylinder with the same stacking properties. The reference flat structure consists of a 5 mm thick aluminum layer ($N_z = 20$) and a 20 mm thick foam layer ($N_z = 50$). The aluminum alloy has properties: $E = 69$ GPa, $\nu = 0.3$, $\mu = 0.1$ %, $\rho = 2768$ kgm^{-3}. The foam layer is modeled as an equivalent fluid according the Johnson–Champoux–Allard rigid

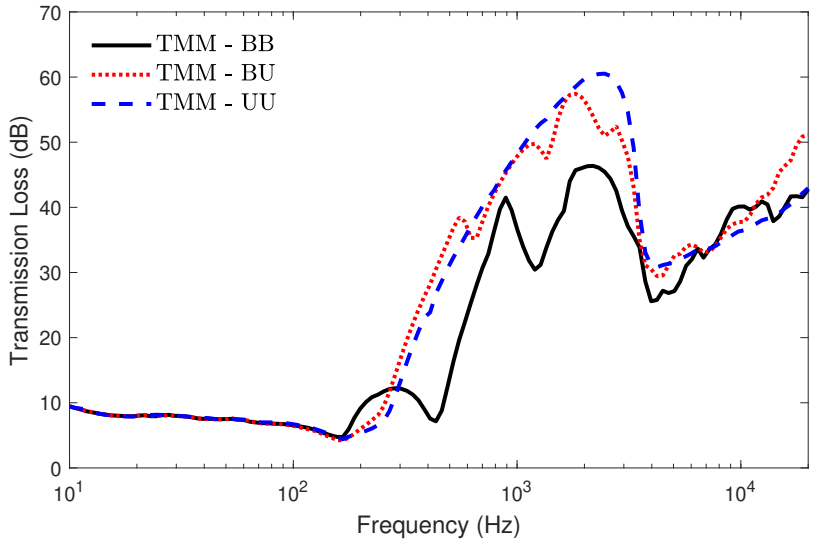

Figure 6: TL for DAF excitation through orthotropic sandwich cylinders ($R = 2.156$ m).

model [31, 35, 36] with properties: $\phi = 0.95$, $\alpha_\infty = 1.42$, $\sigma = 8900$ Nsm^{-4}, $\Lambda = 180$ μm, $\Lambda' = 360$ μm. The IL is evaluated for the flat structure as the difference between the total TL and the TL of the aluminum layer ($\mathrm{TL_{Bare}}$). A DAF excitation is considered. Figure 7 compares the total TL of two cylinders ($R = 1$ m , $R = 8$ m) with the TL obtained as a sum of the analytical (planar layers) TMM calculated IL and the TL of a cylinder consisting of the sole aluminum layer ($\mathrm{TL_{Bare}}$). The analytical TMM IL provides a satisfactory prediction of the total TL of the cylinders in the whole frequency range except around the critical frequency of the bare structure ($\sim$2 kHz) and in the low frequency range for the lowest radius of curvature.

The fourth case concerns a cylinder ($R = 0.1$ m) made up from a non homogeneous periodic cell. The UC is depicted in Figure 8. It consists in a 1 mm thick aluminum shell ($E = 69$ GPa, $\nu = 0.3$, $\mu = 0.1$ %, $\rho = 2768$ kgm^{-3}) of external dimensions $7 \times 7 \times 8$ mm^3 and a soft isotropic elastic material (foam) with a solid inclusion made up from a heavy cube ($\rho = 18000$ kgm^{-3}) with 2

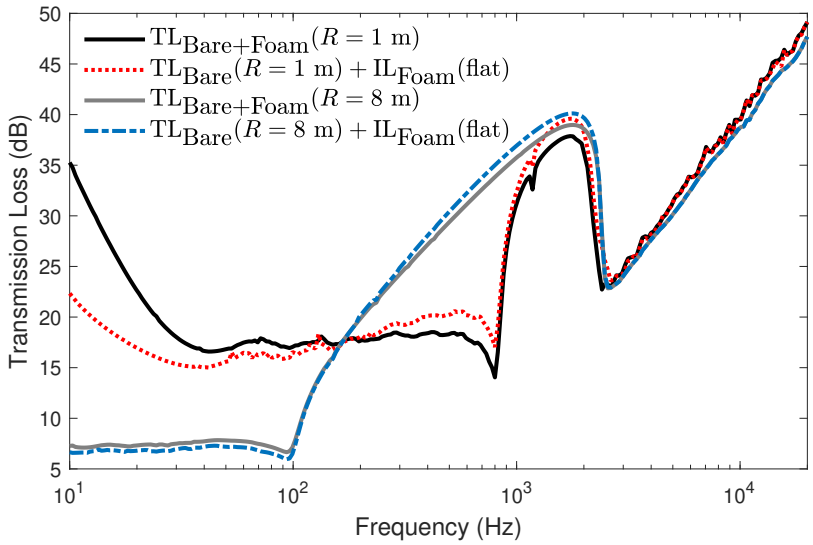

Figure 7: TL for DAF excitation through two cylinders consisting of an aluminum layer and a foam layer.

mm edge. The UC is modeled with hexa27 elements. Figure 9 shows the TL at oblique incidence ($\theta = 45°$, $\Psi = 0°$) through the cylinder for different values of the foam shear modulus, G_{foam}, along with a case with no inclusion (in this case the foam density is increased to achieve the same mass of the other cases). With the inclusion and for $G_{\mathrm{foam}} = 2.5$ kPa the dip related to a resonance of the UC (140 Hz) turns to a peak because of the first resonance of the inclusion and the rest of the TL curve is smooth.

The last case concerns the diffuse field TL through an infinite cylinder ($R =$ 1.2 m) consisting of a 3 mm thick steel layer ($N_z = 20$, $E = 210$ GPa, $\nu = 0.3$, $\mu = 0.1$ %, $\rho = 7800$ kgm^{-3}) and an external layer made up from Helmholtz resonators. The geometry of the resonator is selected to tune its frequency to the ring frequency of the bare cylinder (∼700 Hz). Each resonator consists of a 25 mm long cylindrical neck with internal diameter of 30 mm located inside a 50 mm thick cylindrical cavity with internal diameter of 60 mm. The neck

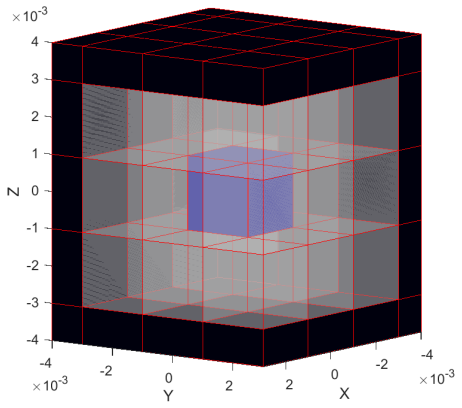

Figure 8: Mesh of a periodic unit cell made of: aluminum shell (black), inner heavy cube (blue), soft foam (gray).

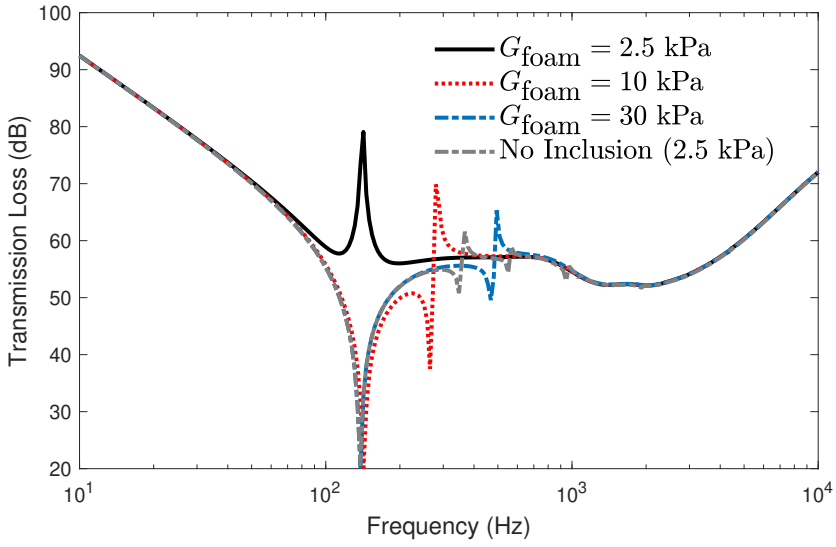

Figure 9: TL at oblique incidence ($\theta = 45°$,$\Psi = 0°$) through a cylinder made up from a non homogeneous unit cell ($R = 0.1$ m).

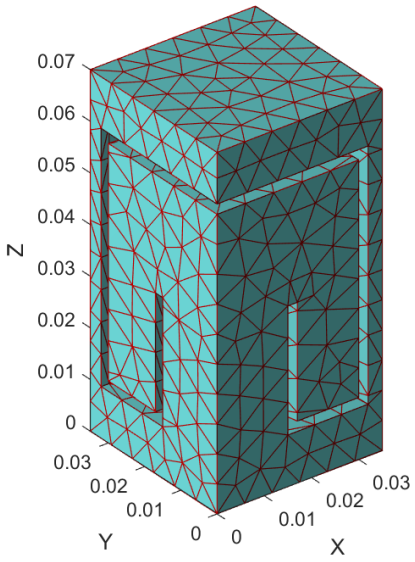

Figure 10: A quarter of the coarse mesh of a Helmholtz resonator.

and the cavity are delimited by 2 mm thick rigid walls. Additional 10 mm thick air layers are located on the top and on the bottom of the resonators. The resonators are 70 mm spaced along both the x-axis and the y-axis and are filled and surrounded by air. A 0.1% of damping is applied to the air inside the resonators. A quarter of a Tetra4 mesh of the layer's UC is depicted in Figure 10. Figure 11 presents the TL at normal incidence of the planar doubly periodic resonator for different meshes. It should be noted that even the coarse mesh makes it possible to capture the physics of the resonator till 5 kHz. As a consequence, the coarse mesh (Figure 10) is used to model the cylinder. Figure 12 shows the TL through the cylinder under a DAF along with the case with no resonators. As expected (the problem is well studied for planar structures) the resonators layer suppresses the dip at the ring frequency ($\sim$700 Hz) and alleviates the dip corresponding to the critical frequency of the bare cylinder ($\sim$4 kHz) thus providing an overall improvement of the transmission performance of the cylinder in the whole frequency range explored.

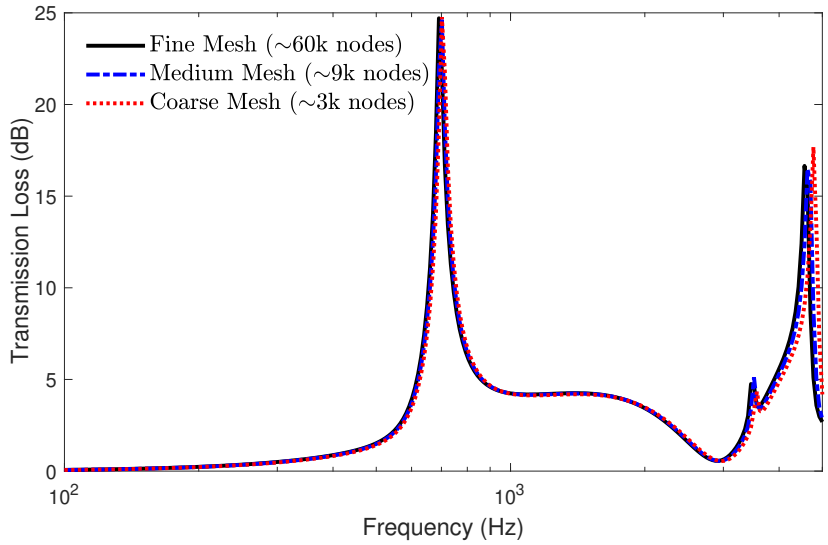

Figure 11: TL at normal incidence of a Helmholtz resonator.

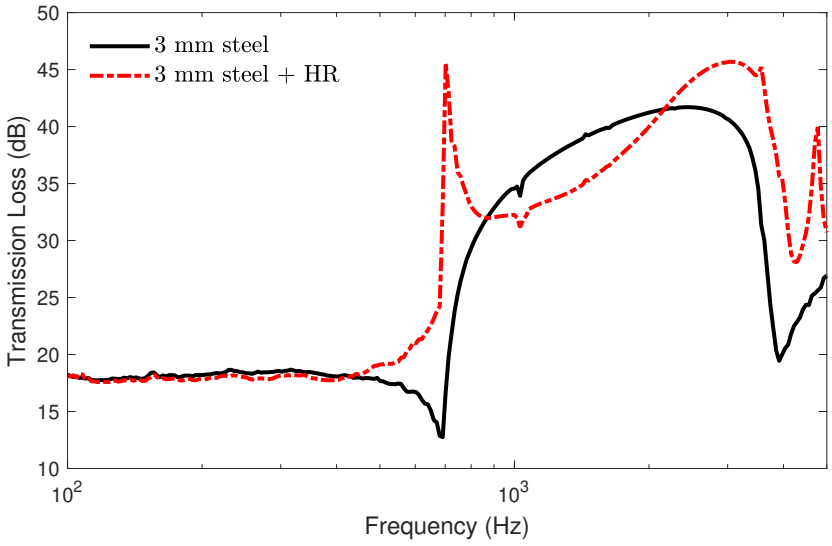

Figure 12: TL for DAF excitation through a 3 mm thick steel cylinder ($R = 1.2$ m) wrapped by Helmholtz Resonators (HR).

4. Conclusions

A general procedure for obtaining the acoustic transfer matrix of a cylindrical layer (fluid, elastic, poroelastic) is described. The procedure involves manipulating the dynamic stiffness matrix of the FE model related to the layer's unit cell. The matrix thus obtained is used in a TMM framework to predict sound transmission through a multilayered cylinder. The proposed procedure allows to exploit the versatility of the TMM and makes it easy to deal with anisotropic, poroelastic and heterogeneous cylinders, avoiding the need for analytical formulations or homogeneous equivalent models.

The accuracy of the model in predicting TLs has been verified by showing agreement with alternative approaches in case of cylinders consisting of homogeneous layers. The practical application of the approach has also been illustrated by: (i) assessing the effect of interface condition on the TL of a sandwich cylinder with a poroelastic core; (ii) testing the validity of a planar structure based insertion loss for the correction of the TL of multilayered cylinders; (iii) designing the unit cell of periodic cylinders in order to suppress a resonance dip or the TL dip at the ring frequency.

The presented TMM ensures a lower computational cost compared to other periodic approaches since each layer can be modeled per se and homogeneous layers may be modeled efficiently with a few finite elements by exploiting the ability to model only a portion of the thickness and by recovering the overall transfer matrix as power of the elementary one. Instead, classical periodic approaches must model the structure with a global unit cell which includes all the layers. Ultimately, the proposed approach could represent an effective acoustic tool for infinite cylinders in a FE analysis environment, due to its versatility and efficiency.

References

[1] C. Boutin, Acoustics of porous media with inner resonators, The Journal of the Acoustical Society of America 134 (6) (2013) 4717–4729. doi:10.1121/1.4824965.

[2] J.-P. Groby, C. Lagarrigue, B. Brouard, O. Dazel, V. Tournat, B. Nennig, Enhancing the absorption properties of acoustic porous plates by periodically embedding helmholtz resonators, The Journal of the Acoustical Society of America 137 (1) (2015) 273–280. doi:10.1121/1.4904534.

[3] O. Doutres, N. Atalla, H. Osman, Transfer matrix modeling and experimental validation of cellular porous material with resonant inclusions, The Journal of the Acoustical Society of America 137 (6) (2015) 3502–3513. doi:10.1121/1.4921027.

[4] L. R. Koval, On sound transmission into a thin cylindrical shell under "flight conditions", Journal of Sound and Vibration 48 (2) (1976) 265–275. doi:10.1016/0022-460X(76)90465-X.

[5] L. R. Koval, On sound transmission into an orthotropic shell, Journal of Sound and Vibration 63 (1) (1979) 51–59. doi:10.1016/0022-460X(79)90376-6.

[6] L. R. Koval, Sound transmission into a laminated composite cylindrical shell, Journal of Sound and Vibration 71 (4) (1980) 523–530. doi:10.1016/0022-460X(80)90724-5.

[7] A. Blaise, C. Lesueur, Acoustic transmission through a 2-d orthotropic multi-layered infinite cylindrical shell, Journal of Sound and Vibration 155 (1) (1992) 95–109. doi:10.1016/0022-460X(92)90648-H.

[8] A. Blaise, C. Lesueur, Acoustic transmission through a" 3-d" orthotropic multi-layered infinite cylindrical shell, part i: Formulation of the problem, Journal of sound and vibration 171 (5) (1994) 651–664. doi:10.1006/jsvi.1994.1147.

[9] A. Blaise, C. Lesueur, Acoustic transmission through a" 3-d" orthotropic multi-layered infinite cylindrical shell, part ii: validation and numerical exploitation for large structures, Journal of Sound and Vibration 171 (5) (1994) 665–680. doi:10.1006/jsvi.1994.1148.

[10] S. Ghinet, N. Atalla, H. Osman, Diffuse field transmission into infinite sandwich composite and laminate composite cylinders, Journal of sound and vibration 289 (4-5) (2006) 745–778. doi:10.1016/j.jsv.2005.02.028.

[11] J. Magniez, J.-D. Chazot, M. A. Hamdi, B. Troclet, A mixed 3d-shell analytical model for the prediction of sound transmission through sandwich cylinders, Journal of Sound and Vibration 333 (19) (2014) 4750–4770. doi:10.1016/j.jsv.2014.04.040.

[12] M. A. Biot, Generalized theory of acoustic propagation in porous dissipative media, The Journal of the Acoustical Society of America 34 (9A) (1962) 1254–1264. doi:10.1121/1.1918315.

[13] K. Daneshjou, H. Ramezani, R. Talebitooti, Wave transmission through laminated composite double-walled cylindrical shell lined with porous materials, Applied Mathematics and Mechanics 32 (6) (2011) 701–718. doi:10.1007/s10483-011-1450-9.

[14] J. Zhou, A. Bhaskar, X. Zhang, The effect of external mean flow on sound transmission through double-walled cylindrical shells lined with poroelastic material, Journal of Sound and Vibration 333 (7) (2014) 1972–1990. doi:10.1016/j.jsv.2013.11.038.

[15] J. Zhou, A. Bhaskar, X. Zhang, Sound transmission through double cylindrical shells lined with porous material under turbulent boundary layer excitation, Journal of Sound and Vibration 357 (2015) 253–268. doi:10.1016/j.jsv.2015.07.014.

[16] H. Ramezani, A. Saghafi, Optimization of a composite double-walled cylindrical shell lined with porous materials for higher sound transmission loss by using a genetic algorithm, Mechanics of Composite Materials 50 (1) (2014) 71–82. doi:10.1007/s11029-014-9394-2.

[17] Y. Liu, C. He, Diffuse field sound transmission through sandwich composite cylindrical shells with poroelastic core and external mean flow, Composite Structures 135 (2016) 383 – 396. doi:10.1016/j.compstruct.2015.09.025.

[18] J.-H. Lee, J. Kim, H.-J. Kim, Simplified method to solve sound transmission through structures lined with elastic porous material, The Journal of the Acoustical Society of America 110 (5) (2001) 2282–2294. doi:10.1121/1.1410967.

[19] J.-M. Mencik, M. Ichchou, Wave finite elements in guided elastodynamics with internal fluid, International Journal of Solids and Structures 44 (7) (2007) 2148 – 2167. doi:10.1016/j.ijsolstr.2006.06.048.

[20] E. Manconi, B. R. Mace, Wave characterization of cylindrical and curved panels using a finite element method, The Journal of the Acoustical Society of America 125 (1) (2009) 154–163. doi:10.1121/1.3021418.

[21] B. R. Mace, E. Manconi, Modelling wave propagation in two-dimensional structures using finite element analysis, Journal of Sound and Vibration 318 (4-5) (2008) 884–902. doi:10.1016/j.jsv.2008.04.039.

[22] J. M. Renno, B. R. Mace, Calculating the forced response of cylinders and cylindrical shells using the wave and finite element method, Journal of Sound and Vibration 333 (21) (2014) 5340–5355. doi:10.1016/j.jsv.2014.04.042.

[23] D. Chronopoulos, B. Troclet, M. Ichchou, J. Lainé, A unified approach for the broadband vibroacoustic response of composite shells, Composites Part

B: Engineering 43 (4) (2012) 1837 – 1846. doi:10.1016/j.compositesb.2012.01.059.

[24] F. Errico, M. Ichchou, S. De Rosa, O. Bareille, F. Franco, The modelling of the flow-induced vibrations of periodic flat and axial-symmetric structures with a wave-based method, Journal of Sound and Vibration 424 (2018) 32–47. doi:10.1016/j.jsv.2018.03.012.

[25] F. Errico, M. Ichchou, F. Franco, S. D. Rosa, O. Bareille, C. Droz, Schemes for the sound transmission of flat, curved and axisymmetric structures excited by aerodynamic and acoustic sources, Journal of Sound and Vibration 456 (2019) 221 – 238. doi:https://doi.org/10.1016/j.jsv.2019.05.041.

[26] C. Droz, O. Robin, M. Ichchou, N. Atalla, Improving sound transmission loss at ring frequency of a curved panel using tunable 3d-printed small-scale resonators, The Journal of the Acoustical Society of America 145 (1) (2019) EL72–EL78. doi:10.1121/1.5088036.

[27] M. J. Kingan, Y. Yang, B. R. Mace, Sound transmission through cylindrical structures using a wave and finite element method, Wave Motiondoi:10.1016/j.wavemoti.2018.07.009.

[28] J. Magniez, M. A. Hamdi, J.-D. Chazot, B. Troclet, A mixed biot–shell analytical model for the prediction of sound transmission through a sandwich cylinder with a poroelastic core, Journal of Sound and Vibration 360 (2016) 203 – 223. doi:10.1016/j.jsv.2015.09.012.

[29] M. Golzari, A. A. Jafari, Sound transmission loss through triple-walled cylindrical shells with porous layers, The Journal of the Acoustical Society of America 143 (6) (2018) 3529–3544. doi:10.1121/1.5041270.

[30] A. Parrinello, G. Ghiringhelli, Transfer matrix representation for periodic planar media, Journal of Sound and Vibration 371 (2016) 196–209. doi:10.1016/j.jsv.2016.02.005.

[31] J. Allard, N. Atalla, Propagation of sound in porous media: modelling sound absorbing materials 2nd edition, John Wiley & Sons, 2009.

[32] M. Abramowitz, I. A. Stegun, Handbook of Mathematical Functions with Formulas, Graphs, and Mathematical Tables, Chap. 9, Dover Publications, 1965.

[33] N. Atalla, R. Panneton, P. Debergue, A mixed displacement-pressure formulation for poroelastic materials, The Journal of the Acoustical Society of America 104 (3) (1998) 1444–1452. doi:10.1121/1.424355.

[34] C. Lesueur, Rayonnement acoustique des structures: vibroacoustique, interactions fluide-structure, Eyrolles, 1988.

[35] D. L. Johnson, J. Koplik, R. Dashen, Theory of dynamic permeability and tortuosity in fluid-saturated porous media, Journal of Fluid Mechanics 176 (1987) 379–402. doi:10.1017/S0022112087000727.

[36] Y. Champoux, J. Allard, Dynamic tortuosity and bulk modulus in air-saturated porous media, Journal of Applied Physics 70 (4) (1991) 1975–1979. doi:10.1063/1.349482.